JACS
JOURNAL OF THE AMERICAN CHEMICAL SOCIETY
Article
pubs.acs.org/JACS

Redesigning the Blue Copper Azurin into a Redox-Active Mononuclear Nonheme Iron Protein: Preparation and Study of Fe(II)-M121E Azurin

Jing Liu,[†,#] Katlyn K. Meier,[‡,#] Shiliang Tian,[†] Jun-long Zhang,[†,▽] Hongchao Guo,[†,⊥] Charles E. Schulz,[§] Howard Robinson,[∥] Mark J. Nilges,[†] Eckard Münck,*[,‡] and Yi Lu*[,†]

[†]Department of Chemistry, University of Illinois at Urbana−Champaign, Urbana, Illinois 61801, United States
[‡]Department of Chemistry, Carnegie Mellon University, Pittsburgh, Pennsylvania 15213, United States
[§]Department of Physics, Knox College, Galesburg, Illinois 61401, United States
[∥]Department of Biology, Brookhaven National Laboratory, Upton, New York 11973, United States

Supporting Information

ABSTRACT: Much progress has been made in designing heme and dinuclear nonheme iron enzymes. In contrast, engineering mononuclear nonheme iron enzymes is lagging, even though these enzymes belong to a large class that catalyzes quite diverse reactions. Herein we report spectroscopic and X-ray crystallographic studies of Fe(II)-M121E azurin (Az), by replacing the axial Met121 and Cu(II) in wild-type azurin (wtAz) with Glu and Fe(II), respectively. In contrast to the redox inactive Fe(II)-wtAz, the Fe(II)-M121EAz mutant can be readily oxidized by Na_2IrCl_6, and interestingly, the protein exhibits superoxide scavenging activity. Mössbauer and EPR spectroscopies, along with X-ray structural comparisons, revealed similarities and differences between Fe(II)-M121EAz, Fe(II)-wtAz, and superoxide reductase (SOR) and allowed design of the second generation mutant, Fe(II)-M121EM44KAz, that exhibits increased superoxide scavenging activity by 2 orders of magnitude. This finding demonstrates the importance of noncovalent secondary coordination sphere interactions in fine-tuning enzymatic activity.

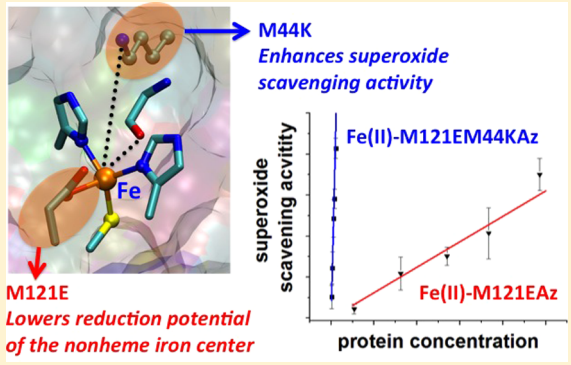

INTRODUCTION

Rational design of metalloproteins is an exciting field where our understanding of native proteins can not only be tested and expanded, but also applied toward engineering less expensive and more robust biocatalysts for many applications.[1−8] While much progress has been made in designing metalloproteins that *structurally* mimic native enzymes, the design of proteins with new and desired functions is still largely limited to heme enzymes or proteins containing small inorganic catalysts.[1,2,7−19] Recent successes in the *de novo* design of enzymes based on helix bundles bearing diiron[20,21] or dirhodium centers[22,23] have been reported. In contrast, limited success has been achieved in the design of mononuclear nonheme iron enzymes,[24,25] even though they belong to a large and important family of enzymes that are active in oxidative stress defenses, oxidation, and oxygenation reactions.[26−28] Such diversity in reaction, combined with the relative abundance of iron and its wide range of accessible oxidation states, has made these enzymes attractive targets for biophysical investigations and synthetic modeling, with the aim of understanding them and developing efficient biomimetic catalysts with earth-abundant metal ions.[26,29−38]

To complement the study of native enzymes and synthetic models, we have chosen the classic electron transfer (ET) protein azurin (Az), from *Pseudomonas aeruginosa*, as a scaffold for biosynthetic modeling. Azurin can easily be purified from *Escherichia coli* in high yields, and the protein is very stable at room temperature. Thus, Az is among the most extensively studied cupredoxins.[39−41] As an ET protein, Az provides a rigid scaffold to position the metal-binding sites as well as to fine-tune its surrounding environment, allowing use of a bottom-up approach to test structural features important for enzymatic activity. The ligand environment in Az comprises His46, His117, and Cys112 in the trigonal plane as well as Met121 and the backbone carbonyl oxygen of Gly45 in the axial positions (Figure 1A).[42]

As the first step to transform this ET protein into a mononuclear nonheme iron enzyme, McLaughlin et al. substituted the native Cu(II) with Fe(II) in wtAz and obtained its crystal structure (Figure 1B).[43] However, the iron occupancy in the crystal was low (35% in two of four chains, with the other two sites being empty), perhaps because Met121 could not

Received: May 29, 2014
Published: July 31, 2014

dx.doi.org/10.1021/ja505410u | J. Am. Chem. Soc. 2014, 136, 12337−12344

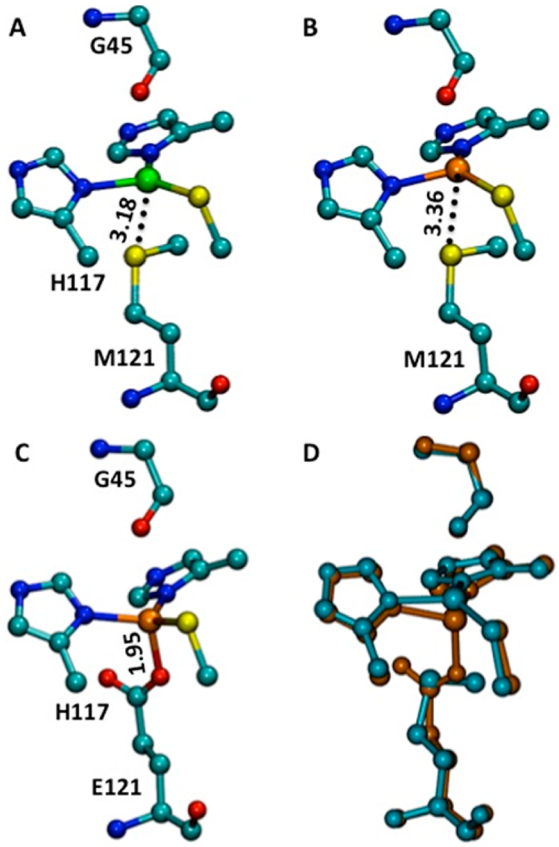

Figure 1. Crystal structures of (A) Chain A of Cu(II)-wtAz. PDB ID: 4AZU. (B) Chain B of Fe(II)-wtAz. PDB ID: 4HZ1. (C) Chain B of Fe(II)-M121EAz. PDB ID: 4QLW. Resolution: 2.0 Å. Distance unit: Å. Color code: C, cyan; S, yellow; N, blue; O, red; Cu, green; Fe, orange. (D) Overlay of chain B of Fe(II)-wtAz (cyan) and Fe(II)-M121EAz (orange).

bind sufficiently strongly to the iron. No redox or enzymatic activity was observed at the Fe(II) center. We hypothesized that replacing the Met121 with Glu, which is not only one carbon atom closer to the metal center than Met, but is also a more common ligand in nonheme iron enzymes, would increase the affinity for iron. Moreover, we expected that the M121E mutation would lower the reduction potential of the iron center through its negative carboxylate charge and would thus convert the redox-inactive Fe(II)-wtAz into a redox-active protein displaying enzymatic activity. Herein we report the design of a nonheme iron binding site in Az and show that the glutamate residue at position 121 plays important roles in conferring higher Fe(II) binding affinity and new redox and superoxide scavenging activity. Furthermore, mutation of the secondary coordination sphere residue Met44 to Lys (M44K) increased the superoxide scavenging activity even further.

RESULTS AND DISCUSSION

M121EAz was expressed and purified from *E. coli* in metal-free apo form following reported procedures.[44] Upon addition of $(NH_4)_2Fe(SO_4)_2$ to apo-M121EAz under anaerobic conditions, development of an absorption at ~315 nm was observed (Figure 2). After passing the protein through a desalting column (PD-10 from GE) to remove free iron, inductively coupled plasma (ICP) analysis confirmed iron incorporation with <1% Zn and <0.1% Cu present in the sample (Table S1).

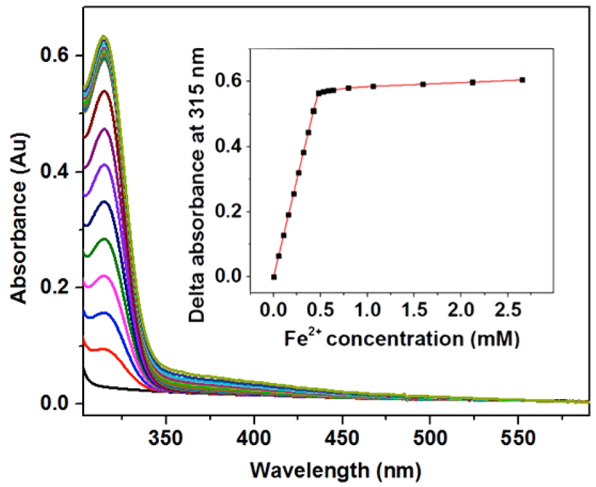

Figure 2. UV−vis absorption spectral increase after successive addition of 0.1−5 equiv of Fe^{2+} to apo-M121EAz (0.48 mM). (Inset) Titration curve monitored by the absorbance maxima at 315 nm.

Based on these results, an extinction coefficient of 1610 M^{-1} cm^{-1} was determined for the absorption at 315 nm. Both the position and extinction coefficient of the absorption band are similar to those observed in cysteinyl coordinated mononuclear nonheme iron enzymes such as Fe(II)-wtAz,[43] superoxide reductase (SOR),[45] and corresponding sulfur-containing small molecular models.[46,47] The features were assigned as sulfur → Fe(II) ligand to metal charge transfer (LMCT) bands. Our results support the successful iron incorporation as well as cysteinyl coordination in M121EAz. The iron incorporation ratio was determined to be 0.9 by titration using ϵ_{280} = 8800 M^{-1} cm^{-1}[48] for apo M121EAz with K_d stronger than 1 μM (Figure 2). Electrospray ionization mass spectrometry (ESI MS) of the protein after iron incorporation displayed a major peak with mass of 14000.0 Da (Figure S2b, calculated mass of Fe + M121EAz: 13999.6 Da), further supporting the monoiron incorporation into the protein.

The purified Fe(II)-M121EAz was successfully crystallized. Its structure, solved at 2.0 Å resolution, showed that the protein is a tetramer consisting of two heterodimers. Subunits A and C are in conformation **1** (Figure S3a) with no observable metal occupancy, similar to the result reported for Fe(II)-wtAz.[43] Subunits B and D are in conformation **2** (Figure S3b) with 100% occupancy, much higher than the 35% occupancy of the corresponding site in Fe(II)-wtAz.[43] This observation demonstrates that the extended carboxylate ligand from Glu121 increases iron binding as designed. While this mutant binds Fe(II) more effectively than Fe(II)-wtAz, the observed sample heterogeneity in Fe(II)-M121EAz may be due to thermodynamic or kinetic effects of Fe(II)−protein or Fe(II)−buffer interactions or some combination of both effects, depending on the mutant.

The major difference between the two conformations is that His117 of subunit A (conformation **1**) is shifted away from the active site by 1.6 Å, with slight movement of His46 and Glu121 (Figure S3c). It has been noted that His117, located in the loop region near the protein surface, is highly flexible as shown in the crystal structures of two of the four subunits of apo-wtAz[49] and Fe(II)-wtAz.[43] In wtAz, this movement has been proposed to be responsible for transferring external metal ions into the binding site during metal incorporation.[49] Thus, under the acidic crystallization condition at pH 5.3, the flexibility of

dx.doi.org/10.1021/ja505410u | J. Am. Chem. Soc. 2014, 136, 12337−12344

His117 in combination with high concentrations of coordinating acetate anions in crystallization buffers would lead to removal of iron in subunits A and C as well as to a decrease in metal/protein ratio in the crystallized form (0.5) compared to that in solution (0.9). To confirm that the acetate buffer played a role in the observed sample heterogeneity, we investigated the effect of adding 100 mM OAc^- to freshly prepared Fe(II)-M121EAz. As shown in Figure S4, at pH 5.3, the 315 nm absorption band decreased with time. On the other hand, this band remained stable at pH 7.8. Therefore, the acetate can remove Fe(II) at low pH, but not high pH, probably because it can compete with the His ligands for the Fe(II) at a low pH where the His can be protonated, while acetate remains deprotonated. No other metal-binding site was observed in any other part of the protein.

In conformation **2** of Fe(II)-M121EAz, for which the iron occupancy is 100%, the primary coordination sphere consists of His117, His46, Cys112, Glu121, and the backbone carbonyl of Gly45 (Figure 1C). Interestingly, the Fe(II)-S(Cys112) bonds in Fe(II)-M121EAz (2.38−2.40 Å) are distinctly longer than the corresponding bonds in Fe(II)-wtAz (2.26−2.29 Å)[43,50] but are similar to those of SOR (2.38−2.45 Å).[51] The Fe(II)-N(His) bond lengths (2.05−2.08 Å) in Fe(II)-M121EAz suggest tight binding. Glu121 coordinates to the Fe(II) in a monodentate mode, similar to that in Cu(II)-M121EAz.[50] The Fe-O(Glu121) distances are 1.95−2.02 Å, which are much shorter than the Fe-S(Met121) distance of 3.36 Å for Fe(II)-wtAz (Figure 1D).[43] These results confirm that the stronger bond between Fe-O(Glu121), as opposed to the Fe-S(Met121) bond in wtAz, is responsible for the more effective binding of Fe(II) by Fe(II)-M121EAz.

Except for cryoreduction by γ-radiation, Fe(II)-wtAz was reported to be inert to most oxidation and reduction attempts.[18,43] In contrast, Fe(II)-M121EAz is readily oxidized by the one-electron oxidant Na_2IrCl_6, as demonstrated by the development of absorption features centered around 600 and 410 nm (Figure 3). This result indicates that the introduction of the negatively charged carboxylate ligand of Glu121 lowers the reduction potential of Fe(II)-M121EAz relative to that of Fe(II)-wtAz, making it oxidizable by Na_2IrCl_6. To determine the redox properties of the Fe(II)-M121EAz mutant quantitatively, we have measured the reduction potential of the iron site using cyclic voltammetry (CV) and obtained +327 ± 9 mV (Figure S5).[52] This value is ∼100 mV higher than that of native SOR (+238 ± 10 mV).[53] Furthermore, in addition to using Na_2IrCl_6 (E_m = +0.87 V), we have measured oxidation of the Fe(II)-M121EAz using 1 equiv of $K_3Fe(CN)_6$ (E_m = +0.358 V) and *N*,*N*,*N*′,*N*′-tetramethyl-*p*-phenylenediamine (TMPD) (E_m = +0.276 V) respectively. Based on UV−vis spectroscopy (see Figure S6), oxidation by $K_3Fe(CN)_6$ was observed, while no oxidation was observed by TMPD, consistent with the reduction potentials measured by CV.

The observation of the new redox activity conferred by the M121E mutation raised the question of whether the Fe(II)-M121EAz displayed any enzymatic activity. Considering that one prominent member of Cys-containing nonheme iron enzymes is SOR, we investigated the superoxide scavenging activity of Fe(II)-M121EAz using the Fridovich method.[54] Reactions of nitrotetrazolium blue chloride (NBT) with superoxide flux generated by xanthine/xanthine oxidase were followed in the presence of catalase and different amounts of Fe(II)-M121EAz. As shown in Figure 4, the reaction rate

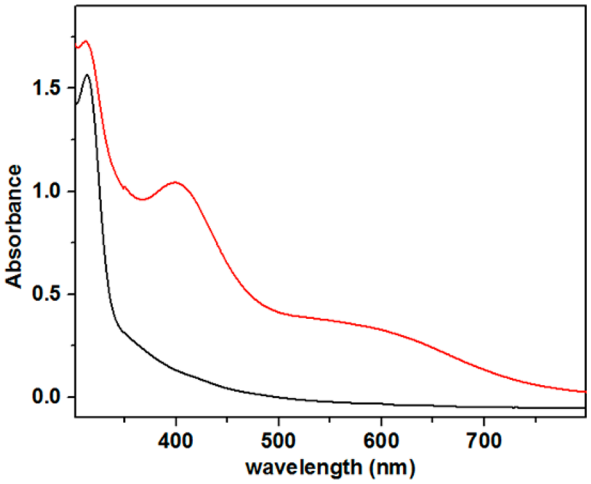

Figure 3. UV−vis spectra of Fe(II)-M121EAz (0.86 mM, black line) and after its oxidation with 1 equiv of Na_2IrCl_6 at room temperature for 10 min (red line).

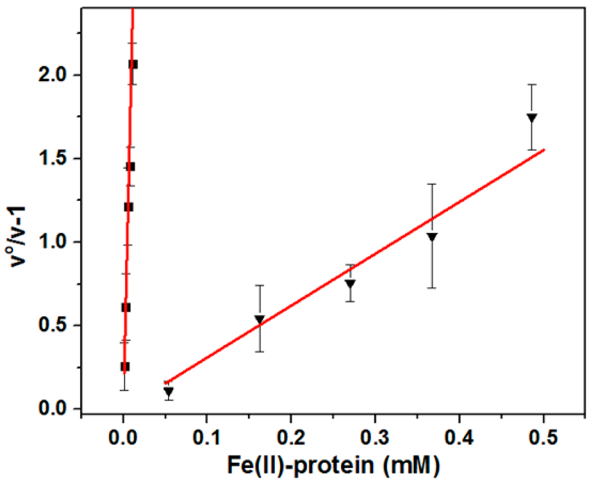

Figure 4. Reactivity toward superoxide by Fridovich test. Triangle: Fe(II)-M121EAz and square: Fe(II)-M121EM44KAz; v°: $\Delta A_{535\ nm}$/min without protein and v: $\Delta A_{535\ nm}$/min with protein.

decreased upon addition of Fe(II)-M121EAz as competitor, with a second-order rate constant of ∼1.8×10^4 M^{-1} s^{-1} at pH 7.8 and 25 °C. This rate is comparable to that reported for the superoxide scavenging reagent NBT (5.94×10^4 M^{-1} s^{-1}).[55] These results indicate that by replacing Met121 with Glu we have succeeded in converting Fe(II)-wtAz into a nonheme iron protein with superoxide scavenging activity.

To elucidate the electronic structure of Fe-M121EAz, we have recorded a series of Mössbauer spectra at 4.2 K in zero-field (B = 0 T) and in applied fields up to B = 9.0 T. The data have been analyzed in the framework of the commonly used spin Hamiltonian:

$$H = D\left[S_z^2 - \frac{S(S+1)}{3} + \left(\frac{E}{D}\right)(S_x^2 - S_y^2)\right] + \beta\vec{S}\cdot\hat{g}\cdot\vec{B} + \vec{S}\cdot\hat{A}\cdot\vec{I} - g_n\beta_n\vec{B}\cdot\vec{I} + H_Q \quad (1)$$

$$H_Q = \frac{eQV_{z'z'}}{12}\left[3I_{z'}^2 - \frac{15}{4} + \eta(I_{x'}^2 - I_{y'}^2)\right] \quad (1a)$$

dx.doi.org/10.1021/ja505410u | J. Am. Chem. Soc. 2014, 136, 12337−12344

In eq 1 we used $S = 5/2$ for Fe(III)-M121EAz and $S = 2$ for Fe(II)-M121EAz. D and E/D are zero-field splitting (ZFS) parameters, $\hat{g}$ is the electronic g-tensor (we use g = 2.00 below), $\hat{A}$ is the ^{57}Fe magnetic hyperfine tensor, and H_Q describes the interaction of the electric field gradient (EFG) with the nuclear quadrupole moment Q; $\eta = (V_{x'x'} - V_{y'y'})/V_{z'z'}$ is the asymmetry parameter of the EFG tensor. The principal axis system of the EFG tensor, $x'y'z'$, is related to xyz by the rotation $(\alpha\beta\gamma)_{EFG}$, where $(\alpha\beta\gamma)$ are Euler angles as used in WMOSS.

The zero-field, 4.2 K Mössbauer spectrum of Fe(II)-M121EAz shown in Figure 5A consists of a doublet with

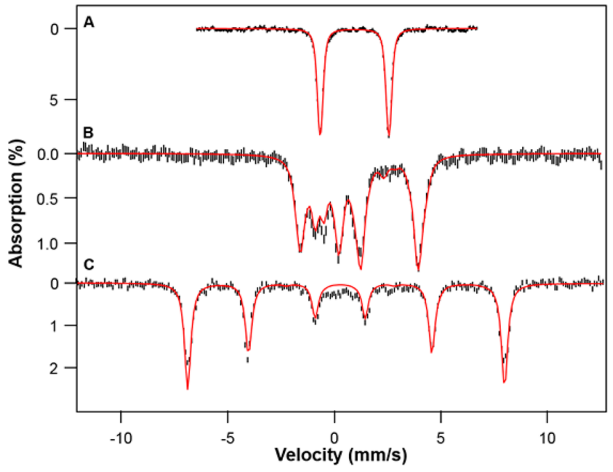

Figure 5. Mössbauer spectra of Fe-M121EAz recorded at 4.2 K in variable magnetic fields applied parallel to the observed γ-radiation. (A) Spectrum of Fe(II)-M121EAz recorded in zero field. The red line is a simulation for $\Delta E_Q = 3.22$ mm/s and $\delta = 0.94$ mm/s. (B) Spectrum of Fe(II)-M121EAz recorded in a 2.0 T field. The red line is a theoretical curve (using WMOSS software) based on the $S = 2$ spin Hamiltonian of eq 1 using the parameters listed in Table 1. (Please note footnote (a) of Table 1.) (C) Zero-field spectrum of Fe(III)-M121EAz obtained by treating an aliquot of the sample of (A) with Na_2IrCl_6. The red line is a spectral simulation of Fe(III)-M121EAz, using an $S = 5/2$ spin Hamiltonian with the parameters listed in Table 1; see also variable field spectra in Figure S8.

quadrupole splitting $\Delta E_Q = 3.22$ mm/s and isomer shift $\delta = 0.94$ mm/s. These parameters are indicative of a high-spin ($S = 2$) Fe(II) site. A spectrum collected at 4.2 K in a parallel-applied magnetic field of 45 mT (not shown) revealed significant magnetic hyperfine broadening of the high-energy feature. This observation indicates that the two *lowest* spin levels of the $S = 2$ multiplet are narrowly spaced (energy gap $\Delta \leq 0.4$ cm^{-1}) and that an electron paramagnetic resonance (EPR) transition might be observable at X-band in both parallel and perpendicular modes. Figure 6A shows an EPR spectrum of Fe(II)-M121EAz recorded in parallel mode (a transverse mode spectrum is shown in Figure S7). This spectrum can be assigned to the "$M_S = \pm 2$" levels of an $S = 2$ system, implying $D < 0$. As discussed in refs 56 and 57, the observed EPR signal depends on $\Delta = 3|D|(E/D)^2$ and g_z (fixed at 2.00 here). Simulations using the software SpinCount[58] yielded the theoretical curve (red) of Figure 6A for $\Delta = 0.328$ cm^{-1}. The shape of the EPR signal depends on Δ, not on D and E separately, and on a parameter describing the distribution of Δ, here $\sigma_{E/D}$.

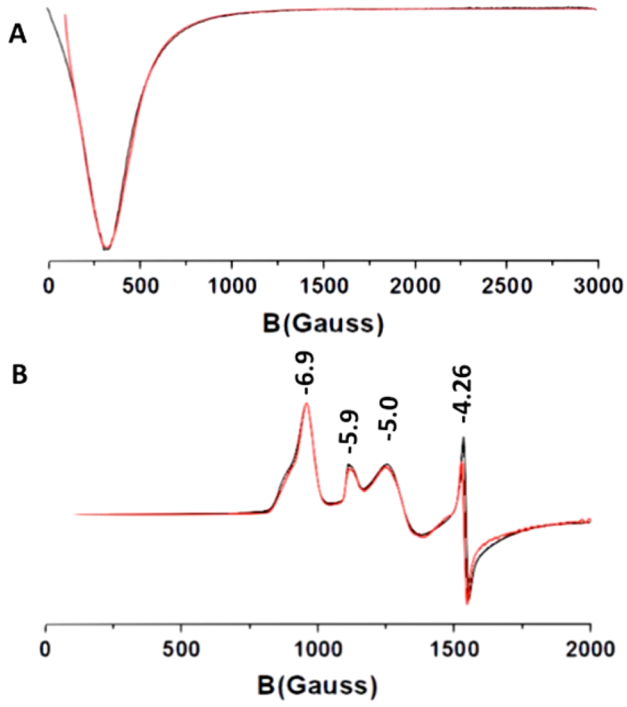

Figure 6. (A) Parallel mode X-band EPR spectrum of Fe(II)-M121EAz recorded at 9 K. The black curve is the experimental spectrum, and the red curve is a simulation generated using the software SpinCount[58] with the parameters listed in Table 1; the parameter E/D (= 0.177) was assumed to have a Gaussian distribution with $\sigma_{E/D} = 0.0055$ (this entails a distribution in Δ). Conditions: microwave power: 2 mW (nonsaturated), microwave frequency: 9.375 GHz, modulation amplitude: 1 mT. (B) Perpendicular mode X-band EPR spectrum of Fe(III)-M121EAz recorded at 10 K. The feature at $g = 4.26$ is a minor contaminant, representing <5% of Fe^{III} present. Conditions: 4 mW, 9.21 GHz, 1 mT. The spectrum was obtained after removing a substantial contribution from Fe(II)-M121EAz.

Treatment of Fe(II)-M121EAz with 2 equiv of Na_2IrCl_6 yields complete conversion to Fe(III)-M121EAz. The 4.2 K, zero field Mössbauer spectrum of the oxidized sample (Figure 5C) reveals a high-spin ($S = 5/2$) ferric component (red line). The observation of a 6-line spectrum with a 3:2:1:1:2:3 intensity pattern indicates that this spectrum is associated with a Kramers doublet for which $g_z \gg g_x, g_y$, a property fitting to the $M_S = \pm 5/2$ doublet. The Mössbauer spectrum is associated with the electronic ground state, and thus the ZFS parameter D is negative. This assignment is confirmed by EPR (see Figures 6B and S9) which revealed two similar species in roughly equal proportions, with $D < 0$ and $E/D = 0.04$ and $E/D = 0.06$. The features between g = 5 and 7 originate from the $M_S = \pm 3/2$ and $\pm 1/2$ excited Kramers doublets. We have recorded variable magnetic field Mössbauer spectra to determine the magnitude of D, thereby avoiding temperature uncertainties inherent in the use of continuous flow EPR cryostats. Analysis of the Mössbauer spectra of Figure S8 yielded $D = -3.0(5)$ cm^{-1}. The spectrum of Figure 5C is not sensitive enough to E/D to distinguish between $E/D = 0.04$ and 0.06, so it was simulated for $E/D = 0.05$.

Recently, McLaughlin et al.[43] reported $\Delta E_Q = -3.19$ mm/s and $\delta = 0.93$ mm/s for Fe(II)-wtAz. The negative ΔE_Q value indicates a low-lying orbital with $\sim d_{z^2}$ symmetry, consistent with a coordination tetrahedron flattened along the z-axis (d_{z^2} is doubly occupied, containing the β electron). As Fe(II)-

dx.doi.org/10.1021/ja505410u | J. Am. Chem. Soc. 2014, 136, 12337−12344

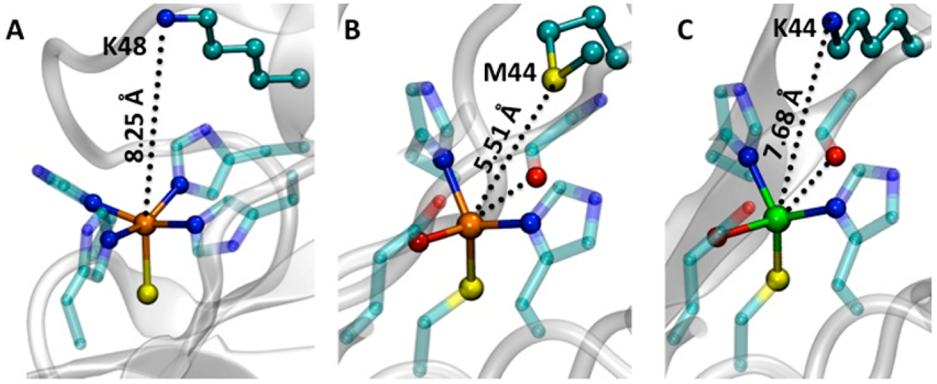

Figure 7. Structure comparison of (A) SOR, PDB ID: 2JI1. (B) Fe(II)-M121EAz, PDB ID: 4QLW. Resolution: 2.0 Å. (C) Cu(II)-M121EM44KAz PDB ID: 4QKT. Resolution: 1.64 Å. Color code: C, cyan; S, yellow; N, blue; O, red; Cu, green; Fe, orange.

Table 1. Mössbauer Parameters of Fe-(II)-M121EAz and Fe(III)-M121EAz

	D (cm^{-1})	E/D	δ (mm/s)	ΔE_Q (mm/s)	η	$A_x/g_n\beta_n$ (T)	$A_y/g_n\beta_n$ (T)	$A_z/g_n\beta_n$ (T)
Fe(II)-M121EAz	{[a]}	{[a]}	0.94 (1)	+3.22 (2)[b]	0.7(2)	−20(10)	−12(3)	−5.3 (2)
Fe(III)-M121EAz	−3.0 (5)	0.05	0.41 (2)	[c]	[c]	−20.0 (5)	−20.0 (5)	−18.4 (1)

[a]The ZFS parameters are constrained from EPR by $\Delta = 3|D|(E/D)^2 = 0.33$ cm^{-1}. Determination of D and E/D requires extensive variable field/variable temperature Mössbauer studies; however, $D < 0$. [b]In the WMOSS simulation the EFG tensor is rotated relative to the ZFS frame by Euler angles $(\alpha\beta\gamma)_{EFG} = (0, 23 \pm 2, 0)$ degrees. [c]Only the projection of the EFG onto the electronic z axis is well determined. The spectrum of Figure 5C yields $eQV_{zz}/2 = +0.30(3)$ mm/s. However, ΔE_Q is confined to +0.2 mm/s < ΔE_Q < +0.8 mm/s.

M121EAz has a tetrahedral coordination as well, we were curious to know whether the M121E mutant also has a d_{z^2} ground state. The 4.2 K, 2.0 T Mössbauer spectrum of Figure 5B reveals a splitting pattern that is left−right reversed compared to that reported for Fe(II)-wtAz,[43] implying that Fe(II)-M121EAz has $\Delta E_Q > 0$, suggesting an $\sim d_{x^2-y^2}$ ground state. In Fe(II)-wtAz, the d_{z^2} and $d_{x^2-y^2}$ orbitals were found to be very close in energy (643 cm^{-1} energy gap), so the reversal observed here is not too surprising.

It is also instructive to compare the Mössbauer parameters of Fe(II)-M121EAz with those reported by Horner et al.[59] for center II of Fe(II)-SOR, namely $\Delta E_Q = 2.82$ mm/s and $\delta = 1.06$ mm/s. While ΔE_Q values of high-spin Fe(II) sites are not very site-specific, isomer shifts are quite sensitive to the coordination geometry. Comparison of the δ values (0.94 vs 1.06 mm/s) indicates substantial differences between the Fe(II)-M121EAz and SOR sites. Inspection of the two structures, shown side by side in Figure 7A,B (for detailed metrics, see Figure S10), shows that Fe(II)-SOR has a square pyramidal geometry, while Fe(II)-M121EAz has a distorted tetrahedral ligand environment. Perhaps most significantly, both centers have a cysteinate ligand coordinated *trans* to the putative O_2^- binding site, a feature which may explain why Fe(II)-M121EAz displays superoxide scavenge activity.

Even though we have converted a redox-inactive Fe(II)-wtAz into a redox-active Fe(III)-M121EAz with superoxide scavenging capability, the activity is still substantially lower than that of native SOR (8×10^8 M^{-1} s^{-1}).[60] Therefore, we set out to improve the activity of this mutant, directing our attention to the secondary coordination sphere. It has been reported[60] that a Lys residue (Lys48) near the axial position of the iron center in SOR is critical for the reaction with superoxide (Figure 7A), as it may guide the binding superoxide to the iron center.[61] Mutation of Lys48 to Ile resulted in ∼20-fold decrease in activity compared to that of wtSOR.[60] The crystal structure of Fe(II)-M121EAz reveals that Met44 is 5.51 Å away from the iron center (Figure 7B). Therefore, an additional M44K mutant was designed based on structural comparison with SOR. Mutation of Met44 to Lys resulted in Fe(II)-M121EM44KAz that displayed a LMCT band at 319 nm with K_d stronger than 1 μM, similar to that of Fe(II)-M121EAz (Figure S11). The crystal structure of Cu(II)-M121EM44KAz shows that the newly introduced Lys is 7.7−8.0 Å from the metal center, analogous to the Lys residue in SOR (Figures 7C and S13). The reduction potential of Fe(II)-M121EM44KAz was measured by CV to be +320 ± 10 mV,[52] within the error range comparable to that of Fe(II)-M121EAz (Figure S14). Oxidation experiments with Na_2IrCl_6, $K_3Fe(CN)_6$ and TMPD gave results similar to those of Fe(II)-M121EAz (Figure S15). Interestingly, the rate constant of Fe(II)-M121EM44KAz with superoxide was determined to be $\sim 1.1 \times 10^6$ M^{-1} s^{-1}, which is 2 orders of magnitude higher than that observed for Fe(II)-M121EAz (Figure 4). Since the reduction potential of this mutant is about the same as the one without the M44K mutation, ruling out reduction potential as a factor responsible for the difference in activity, one explanation for the enhanced activity is that the side chain of the positively charged Lys residue assists in guiding the negatively charged superoxide anions toward the Fe(II) center in Fe(II)-M121EM44KAz. Another possible explanation is that Lys may potentially form a hydrogen bond to the superoxo substrate that is bound to the Fe center, thus promoting activity. To determine the stability of both Fe(II)-M121EAz and Fe(II)-M121EM44KAz within the time frame of the activity assay, we measured the UV−vis spectra of both mutants in the assay buffer of 50 mM potassium phosphate (pH 7.8) containing 0.1 mM EDTA and found that the LMCT bands of both mutants remained stable throughout the NBT test time frame (Figure S4), indicating that the superoxide scavenging activity is associated with the protein metallo-cofactor, not with leaked free iron.

dx.doi.org/10.1021/ja505410u | J. Am. Chem. Soc. 2014, 136, 12337−12344

CONCLUSION

In summary, by replacing Met121 with Glu and native Cu(II) with Fe(II), we have engineered a nonheme iron-binding site in the ET protein Az producing a 2N(His)-1O(Glu)-1S(Cys) coordination sphere. The resulting M121EAz mutant has a higher affinity for Fe(II) than wtAz. In contrast to the redox-inactive Fe(II)-wtAz, Fe(II)-M121EAz is readily oxidized by Na_2IrCl_6 and, more interestingly, displays superoxide scavenging activity. Mössbauer and EPR spectroscopies, along with comparisons of X-ray structures, have been used to elucidate the similarities and differences between these two proteins. While the spectroscopic data reported here are part of an ongoing study, it should be noted that the EPR spectrum of Fe(II)-M121EAz is readily observed in both parallel and perpendicular modes, making it a convenient monitor for reactivity studies. Additionally, the secondary sphere mutation M44K, which was inspired by structural comparison with SOR, yielded a rate constant toward superoxide that was increased by 2 orders of magnitude. This finding demonstrates the importance of noncovalent second sphere interactions for fine-tuning enzymatic activity. While these initial findings are interesting, comprehensive studies, involving several spectroscopic techniques in conjunction with quantum chemical computations, are required to provide a correlation between the electronic structures of both mutants and their superoxide scavenging activity. Such studies as well as a search for intermediates have been initiated in our laboratories.

EXPERIMENTAL SECTION

Materials. Nirotetrazolium blue chloride (NBT), xanthine, Fe-$(NH_4)_2(SO_4)_2{\cdot}6H_2O$, FeNa(EDTA), Na_2IrCl_6, $K_3Fe(CN)_6$, TMPD, chelex-100 sodium form, and catalase from Bovine liver (3809 units/mg) were purchased from Sigma-Aldrich Chemical Co. Xanthine oxidase from buffer milk (20 mg/mL) was purchased from EMD Chemicals, Inc. The water used in all experiments was purified by a Milli-Q system (Millipore, Bedford, MA, USA). All buffers were cleaned by chelex-100 sodium form. All other chemical reagents were obtained from Fisher Scientific Inc. and used without further purification.

Protein Purification. M121EAz and M121EM44KAz were expressed and purified as reported previously.[44] Homogeneity of the apo protein was achieved by passing through a size exclusion column at the last step.

Fe(II) Incorporation. Fe(II) incorporation was carried out under anaerobic conditions. Apo Az mutant in Tris·HCl (25 mM, pH 7.8) was degassed with N_2 and transferred into a glovebag. Concentrations of the protein were measured based on the absorption at 280 nm (extinction coefficient of 8800 $M{\cdot}cm^{-1}$ was used),[48] and 0.9−1 equiv of $Fe(NH_4)_2(SO_4)_2{\cdot}6H_2O$ was added slowly to the protein solution during stirring. The mixture was stirred at 5 °C under N_2 atmosphere for 2 h to ensure complete incorporation of Fe(II). Excess iron salt was removed by a desalting PD-10 column in the glovebag to afford the ferrous holo-protein. The resulting Fe(II)-M121EAz was characterized by UV−vis spectrometry, syringe-pump electrospray ionization mass spectrometry, and inductively coupled plasma analysis (ICP). The Fe(II)-M121EAz concentrations were calculated based on $\varepsilon_{315\ nm}$ of 1610 $M^{-1}\ cm^{-1}$ determined by ICP, and the same extinction coefficient was used for the 319 nm peak of the Fe(II)-M121EM44KAz mutant.

Electron Spray Ionization Mass Spectrometry (ESI MS). Mass spectra of proteins were measured with a Waters Quattro II spectrometer operating in positive-ion mode. Protein samples were exchanged into acidic ammonium acetate buffer to make the final concentration between 10 and 20 μM. The injection syringe was prewashed with 20% formic acid (20% v/v aqueous solution), and 10 μL protein was injected into 50% CH_3CN/H_2O mobile phase with 50 μL/min flow rate. The resulting spectra were integrated over the first minute of detection. The mass spectra were collected from 500 to 2000 m/z and were deconvoluted using the MassLinx software package with a 1 Da resolution and a 10,000−20,000 Da calculation window. Syringe pump mass spectra were used to detect interactions weaker than covalent bonding, such as metal cofactors coordinated by the protein scaffold. Protein samples were exchanged into ammonium acetate buffer (pH 5.1−6.3, 10 mM) to make the final concentration between 0.1 and 0.2 mM. The injection syringe was prewashed with MeOH. The protein sample was loaded into the syringe and was directly injected into the spectrometer by syringe pump at a rate of 5 μL/min. The mass spectra were collected from 500 to 2050 m/z and were deconvoluted using the MassLinx software package with a 1 Da resolution and a 10,000−20,000 Da calculation window.

EPR Spectroscopy. The EPR spectra were collected and analyzed, throughout the development of the project, in two different laboratories. The EPR spectra of Figures 6B and S9 were recorded at the University of Illinois and those of Figures 6A and S7 at Carnegie Mellon University.

Fe(II)-M121EAz Sample Preparation and EPR Data Collection. A 200 μL of Fe(II)-M121EAz (2 mM) in in Mes (50 mM, pH 5.5) was mixed thoroughly with 50 μL of glycerol, transferred to EPR tube, and frozen in liquid N_2 for data collection. The perpendicular (9.66 GHz) and parallel (9.38 GHz) mode X-band EPR spectra of Fe(II)-M12EAz shown in Figures 6A and S7 were recorded at Carnegie Mellon University on a Bruker E500 spectrometer equipped with an Oxford ESR910 liquid helium cryostat for low-temperature measurements and a bimodal cavity (Bruker ER4116DM) for generation of microwave fields parallel and perpendicular to the static field. The SpinCount software[58] used for EPR analysis was provided by Dr. Michael P. Hendrich of Carnegie Mellon University. Weak signals in the g = 2 region were observed in the Fe(II)-M121EAz spectrum (Figure S7) and are attributed to ∼1 μM Cu(II) contamination from the protein preparation.

Fe(III)-M121EAz Sample Preparation and EPR Data Collection. An 1 equiv of Na_2IrCl_6 (10.6 μL, 100 mM) was added slowly to Fe(II)-M121EAz (5.6 mM, 189.4 μL) in Mes (50 mM, pH 5.5) under stirring. The resulting mixture was reacted at room temperature for 8.5 min before mixing with 50 μL glycerol (which took ∼0.5 min) and freezing in liquid N_2. The final concentration of total Fe was 4.24 mM. Three Fe(II)-M121EAz samples were prepared similarly without Na_2IrCl_6, containing 0.42 mM (10%) and 0.85 mM (20%) ferrous protein, respectively. Five Fe(III)Na(ETDA) samples were prepared by diluting 50 mM stock solution in Mes (50 mM, pH 5.5) with the same buffer and mixing with 20% glycerol, and the final concentrations of Fe(III) were 1, 2, 3, 4, and 5 mM, respectively. X-band EPR was recorded at 10 K on a Varian E-line Century Series EPR spectrometer (E102 Microwave Bridge) fitted with a liquid He coldfinger. Double integration of the Fe(III)Na(EDTA) sample after gain correction gave a standard plot for area and spin concentration.[62] The total spin density of the Na_2IrCl_6 oxidized sample was calculated to be 82% of the starting ferrous sample by double integration of the spectra. Fitting of spectra was done with the simulation program SIMPIPM.[63] The remaining ferrous concentration was estimated by comparison with the two Fe(II)-M121EAz samples (Figure S9). A control sample of excess Na_2IrCl_6 was scanned for comparison with the g = 2 region of the Fe(III)-M121EAz spectrum (Figure S9).

Mössbauer Spectroscopy. $^{57}Fe^{2+}$ incorporation was carried out with $^{57}FeCl_2$ following procedures described above. The ^{57}Fe(II)-M121EAz was buffered in 50 mM MES at pH 5.5.

Mössbauer spectra shown in Figure 5 of the main text were recorded at Carnegie Mellon University with two spectrometers, using Janis Research (Wilmington, MA) SuperVaritemp dewars that allow studies in applied magnetic fields up to 8.0 T in the temperature range from 1.5 to 200 K. Mössbauer spectral simulations were performed using the WMOSS software package (SEE Co, Edina, MN). Isomer shifts are quoted relative to Fe metal at 298 K.

Mössbauer spectra shown in Figure S8 were recorded at Knox College at 4.2 K in applied fields of 0, 1, 5, and 9 T. Mössbauer

spectral simulations were performed using a proprietary nonlinear least-squares fitting program.

X-ray Crystallography. The Fe(II)-M121EAz was crystallized based on apo-Az crystallization condition.[49] The Fe(II)-M121EAz (2 mM) was mixed with crystallization buffer containing $(NH_4)_2SO_4$ (3.25 M), $LiNO_3$ (0.1 M), NaOAc (0.1 M) at pH 5.3 in 3:3, 3:2, and 3:1 ratio, respectively, on a silica slide and equilibrate over 500 μL well buffer using hanging drop method at 5 °C. Colorless block crystals were obtained after 2−3 weeks. The crystals were dipped in cryo-buffer containing 70% of well buffer and 30% of glycerol before mounting and frozen in liquid N_2 for diffraction data collection and analysis. Crystallographic parameters are shown in Table S2. Diffraction data were collected using 1.0750 Å as wavelengths of data collection at the Brookhaven National Synchrotron Light Source X29 beamline. All data were integrated using the program HKL2000.[64] The crystal structure was solved by the molecular replacement method using MOLREP in the CCP4 Suite.[65] Refinement was performed using Refmac[66] in the CCP4 Suite and Coot.[67]

The Cu(II)-M121EM44KAz was crystallized following literature conditions.[44] 3 uL of approximately 20 mg/mL apo-M121EM44KAz in NaOAc (100 mM, pH 5.6) were mixed with a well buffer containing PEG 4000 (25%), $LiNO_3$ (100 mM), $CuSO_4$ (10 mM), and Tris (100 mM, pH 8.0) in 3:3, 3:2 and 3:1 ratio, respectively, on a silica slide and allowed to equilibrate over 300 μL well buffer using hanging drop method at 5 °C. Light-gray block crystals were grown within 3 days. The crystals were dipped in cryo-buffer containing 70% of well buffer and 30% of glycerol before mounting and frozen in liquid N_2 for diffraction data collection and analysis. Crystallographic parameters are shown in Table S3. Diffraction data were collected using 1.0750 Å as wavelengths of data collection at the Brookhaven National Synchrotron Light Source X29 beamline. All data were integrated using the program HKL2000.[64] The crystal structure was solved by the molecular replacement method using PhaserMR in the PHENIX Suite.[68] Refinement was performed using phenix.refine in the PHENIX Suite[68] and Coot.[67]

Superoxide Activity Assay. Superoxide scavening activity was determined by the Fridovich method using nirotetrazolium blue chloride (NBT) reduction.[54] Superoxide was generated enzymatically by the xanthine−xanthine oxidase system and spectrophotometrically detected by monitoring the formation of the NBT reduction at 535 nm. All measurements were carried out in 1 cm cuvettes at 25 °C controlled by a NESLAB Digital Plus RTE 7 water bath circulator and monitored by an Agilent 8453 UV−vis spectrometer. The reaction system was in phosphate buffer KPi (pH 7.8, 50 mM) containing 0.1 mM EDTA to stabilize xanthine oxidase. 7 μL xanthine oxidase was diluted by 193 μL KPi (50 mM, pH 7.8) containing 0.1 mM EDTA as stock solution. The reaction mixture was composed of xanthine (0.5 mM, 60 μL), catalase (2 μL, 5×10^4 units/mL, to decompose possible H_2O in the reaction system and avoid side reactions with Az mutants), NBT (10 μL, 1.5 mM), and reaction buffer with or without investigated Az mutants to make 140 μL solution. 10 μL xanthine oxidase stock solution was added to the reaction mixture and mixed thoroughly with 200 μL Pipetman to initiate the reaction. The NBT reduction rate was measured both in the presence and absence of the ferrous Az mutants for 250 s for each concentration. The rate without ferrous Az is defined as v^o, and the one with Az is v. Five concentrations were tested for each mutant for three times, and $[(v^o/v) - 1]$ values were plotted against protein concentration to estimate the concentration which causes 50% of inhibition of NBT reduction $((v^o/v) - 1 = 1)$. The reaction rate with superoxide was estimated by $[Az]^{50}$*rate = [NBT]*$rate^{NBT}$, [NBT] = 0.1 mM, $rate^{NBT} = 5.94 \times 10^4$ M^{-1} s^{-1},[55] $[Az]^{50}$ is the concentration when $(v^o/v) - 1 = 1$.

Electrochemical Measurements. The reduction potential of each mutant was determined by CV using a CH Instruments 617A potentiostat equipped with a picoamp booster and a Faraday cage. A pyrolytic graphite edge electrode was polished, and 2−3 μL of protein solution was applied directly to the electrode following previously described methods.[52] After a short incubation time, the electrode was immersed in MOPS (pH 7.0, 50 mM) with 100 mM $NaNO_3$ on ice before data collection. Each protein was then sampled on two different electrodes with or without coabsorbent didecyldimethylammonium bromide (DDAB) between −200 mV and 500 mV. The reduction potentials were measured against Ag/AgCl and converted to SHE.

■ ASSOCIATED CONTENT

Supporting Information

Additional spectroscopic data. This material is available free of charge via the Internet at http://pubs.acs.org.

■ AUTHOR INFORMATION

Corresponding Authors

emunck@cmu.edu

yi-lu@illinois.edu

Present Addresses

[▽]Beijing National Laboratory for Molecular Sciences, State Key Laboratory of Rare Earth Materials Chemistry and Applications, College of Chemistry and Molecular Engineering, Peking University, Beijing 100871, P.R. China.

[⊥]Department of Applied Chemistry, China Agricultural University, Beijing 100193, China.

Author Contributions

[#]These authors contributed equally.

Notes

The authors declare no competing financial interest.

■ ACKNOWLEDGMENTS

We wish to thank Ms. Rebecca L. Keller, Professor Carsten Krebs, Professor J. Martin Bollinger, Jr. from The Pennsylvania State University for initial investigations of the protein using Mössbauer spectroscopy, Mr. Yi-Gui Gao from University of Illinois at Urbana-Champaign for initial investigations of the protein crystal structure, and Ms. Parisa Hosseinzadeh from University of Illinois at Urbana-Champaign for help with the CV data collection and analysis. This work was supported by the National Science Foundation under awards CHE1413328 (YL) and CHE 1305111(EM).

■ REFERENCES

(1) Lu, Y.; Yeung, N.; Sieracki, N.; Marshall, N. M. *Nature* **2009**, *460*, 855.

(2) Lu, Y.; Berry, S. M.; Pfister, T. D. *Chem. Rev.* **2001**, *101*, 3047.

(3) Goodman, C. M.; Choi, S.; Shandler, S.; DeGrado, W. F. *Nat. Chem. Biol.* **2007**, *3*, 252.

(4) Ghosh, D.; Pecoraro, V. L. *Curr. Opin. Chem. Biol.* **2005**, *9*, 97.

(5) Schueler-Furman, O.; Wang, C.; Bradley, P.; Misura, K.; Baker, D. *Science* **2005**, *310*, 638.

(6) Gibney, B. R. *Protein Folding Met. Ions* **2011**, 227.

(7) Abe, S.; Ueno, T.; Watanabe, Y. *Top. Organomet. Chem.* **2009**, *25*, 25.

(8) Köhler, V.; Wilson, Y. M.; Lo, C.; Sardo, A.; Ward, T. R. *Curr. Opin. Biotechnol.* **2010**, *21*, 744.

(9) Yeung, N.; Lin, Y.-W.; Gao, Y.-G.; Zhao, X.; Russell, B. S.; Lei, L.; Miner, K. D.; Robinson, H.; Lu, Y. *Nature* **2009**, *462*, 1079.

(10) Lu, Y.; Valentine, J. S. *Curr. Opin. Struct. Biol.* **1997**, *7*, 495.

(11) Lu, Y. *Curr. Opin. Chem. Biol.* **2005**, *9*, 118.

(12) Lu, Y. *Angew. Chem., Int. Ed.* **2006**, *45*, 5588.

(13) Lu, Y. *Inorg. Chem.* **2006**, *45*, 9930.

(14) Kurtz, D. M., Jr. *Dalton Trans.* **2007**, 4115.

(15) Clark, K. M.; van der Donk, W. A.; Lu, Y. *Methods Enzymol.* **2009**, *462*, 97.

(16) Lu, Y.; Garner, D. K.; Zhang, J.-l. *Wiley Encycl. Chem. Biol.* **2009**, *1*, 124.

(17) Marshall, N. M.; Garner, D. K.; Wilson, T. D.; Gao, Y.-G.; Robinson, H.; Nilges, M. J.; Lu, Y. *Nature* **2009**, *462*, 113.

(18) Davydov, R. M.; McLaughlin, M. P.; Bill, E.; Hoffman, B. M.; Holland, P. L. *Inorg. Chem.* **2013**, *52*, 7323.
(19) Petrik, I. D.; Liu, J.; Lu, Y. *Curr. Opin. Chem. Biol.* **2014**, *19*, 67.
(20) Reig, A. J.; Pires, M. M.; Snyder, R. A.; Wu, Y.; Jo, H.; Kulp, D. W.; Butch, S. E.; Calhoun, J. R.; Szyperski, T. G.; Solomon, E. I.; DeGrado, W. F. *Nat. Chem.* **2012**, *4*, 900.
(21) Calhoun, J. R.; Nastri, F.; Maglio, O.; Pavone, V.; Lombardi, A.; DeGrado, W. F. *Biopolymers* **2005**, *80*, 264.
(22) Popp, B. V.; Ball, Z. T. *J. Am. Chem. Soc.* **2010**, *132*, 6660.
(23) Chen, Z.; Vohidov, F.; Coughlin, J. M.; Stagg, L. J.; Arold, S. T.; Ladbury, J. E.; Ball, Z. T. *J. Am. Chem. Soc.* **2012**, *134*, 10138.
(24) Farinas, E.; Regan, L. *Protein Sci.* **1998**, *7*, 1939.
(25) Pinto, A. L.; Hellinga, H. W.; Caradonna, J. P. *Proc. Natl. Acad. Sci. U. S. A.* **1997**, *94*, 5562.
(26) Costas, M.; Mehn, M. P.; Jensen, M. P.; Que, L., Jr. *Chem. Rev.* **2004**, *104*, 939.
(27) Solomon, E. I.; Brunold, T. C.; Davis, M. I.; Kemsley, J. N.; Lee, S.-K.; Lehnert, N.; Neese, F.; Skulan, A. J.; Yang, Y.-S.; Zhou, J. *Chem. Rev.* **2000**, *100*, 235.
(28) van der Donk, W. A.; Krebs, C.; Bollinger, J. M., Jr. *Curr. Opin. Struct. Biol.* **2010**, *20*, 673.
(29) Tshuva, E. Y.; Lippard, S. J. *Chem. Rev.* **2004**, *104*, 987.
(30) Girerd, J.-J.; Banse, F.; Simaan, A. J. *Struct. Bonding (Berlin, Ger.)* **2000**, *97*, 145.
(31) Que, L. *Acc. Chem. Res.* **2007**, *40*, 493.
(32) Cho, J.; Sarangi, R.; Nam, W. *Acc. Chem. Res.* **2012**, *45*, 1321.
(33) Kovacs, J. A.; Brines, L. M. *Acc. Chem. Res.* **2007**, *40*, 501.
(34) McQuilken, A. C.; Goldberg, D. P. *Dalton Trans.* **2012**, *41*, 10883.
(35) Berry, J. F.; Bill, E.; Bothe, E.; DeBeer George, S.; Mienert, B.; Neese, F.; Wieghardt, K. *Science* **2006**, *312*, 1937.
(36) Ye, S.; Neese, F. *Curr. Opin. Chem. Biol.* **2009**, *13*, 89.
(37) MacBeth, C. E.; Golombek, A. P.; Young, V. G., Jr.; Yang, C.; Kuczera, K.; Hendrich, M. P.; Borovik, A. S. *Science* **2000**, *289*, 938.
(38) Braymer, J. J.; O'Neill, K. P.; Rohde, J.-U.; Lim, M. H. *Angew. Chem., Int. Ed.* **2012**, *51*, 5376.
(39) Fernández, C. O.; Vila, A. J. *ACS Symp. Ser.* **2003**, *858*, 287.
(40) Messerschmidt, A. *Struct. Bonding (Berlin, Ger.)* **1998**, *90*, 37.
(41) Kolczak, U.; Dennison, C.; Messerschmidt, A.; Canters, G. W. *Handb. Metalloproteins* **2001**, *2*, 1170.
(42) Nar, H.; Messerschmidt, A.; Huber, R.; Van de Kamp, M.; Canters, G. W. *J. Mol. Biol.* **1991**, *221*, 765.
(43) McLaughlin, M. P.; Retegan, M.; Bill, E.; Payne, T. M.; Shafaat, H. S.; Peña, S.; Sudhamsu, J.; Ensign, A. A.; Crane, B. R.; Neese, F.; Holland, P. L. *J. Am. Chem. Soc.* **2012**, *134*, 19746.
(44) Lancaster, K. M.; George, S. D.; Yokoyama, K.; Richards, J. H.; Gray, H. B. *Nat. Chem.* **2009**, *1*, 711.
(45) Jovanović, T.; Ascenso, C.; Hazlett, K. R. O.; Sikkink, R.; Krebs, C.; Litwiller, R.; Benson, L. M.; Moura, I.; Moura, J. J. G.; Radolf, J. D.; Huynh, B. H.; Naylor, S.; Rusnak, F. *J. Biol. Chem.* **2000**, *275*, 28439.
(46) McDonald, A. R.; Van Heuvelen, K. M.; Guo, Y.; Li, F.; Bominaar, E. L.; Münck, E.; Que, L. *Angew. Chem., Int. Ed.* **2012**, *51*, 9132.
(47) Namuswe, F.; Kasper, G. D.; Narducci Sarjeant, A. A.; Hayashi, T.; Krest, C. M.; Green, M. T.; Moënne-Loccoz, P.; Goldberg, D. P. *J. Am. Chem. Soc.* **2008**, *130*, 14189.
(48) Tennent, D. L.; McMillin, D. R. *J. Am. Chem. Soc.* **1979**, *101*, 2307.
(49) Nar, H.; Messerschmidt, A.; Huber, R.; Van de Kamp, M.; Canters, G. W. *FEBS Lett.* **1992**, *306*, 119.
(50) Karlsson, B. G.; Tsai, L.-C.; Nar, H.; Sanders-Loehr, J.; Bonander, N.; Langer, V.; Sjölin, L. *Biochemistry* **1997**, *36*, 4089.
(51) Katona, G.; Carpentier, P.; Nivière, V.; Amara, P.; Adam, V.; Ohana, J.; Tsanov, N.; Bourgeois, D. *Science* **2007**, *316*, 449.
(52) Jeuken, L. J. C.; Armstrong, F. A. *J. Phys. Chem. B* **2001**, *105*, 5271.
(53) Clay, M. D.; Jenney, F. E., Jr.; Hagedoorn, P. L.; George, G. N.; Adams, M. W. W.; Johnson, M. K. *J. Am. Chem. Soc.* **2002**, *124*, 788.
(54) Beauchamp, C.; Fridovich, I. *Anal. Biochem.* **1971**, *44*, 276.
(55) Liao, Z. R.; Zheng, X. F.; Luo, B. S.; Shen, L. R.; Li, D. F.; Liu, H. L.; Zhao, W. *Polyhedron* **2001**, *20*, 2813.
(56) Hendrich, M. P.; Debrunner, P. G. *Biophys. J.* **1989**, *56*, 489.
(57) Gupta, R.; Lacy, D. C.; Bominaar, E. L.; Borovik, A. S.; Hendrich, M. P. *J. Am. Chem. Soc.* **2012**, *134*, 9775.
(58) Golombek, A. P.; Hendrich, M. P. *J. Magn. Reson.* **2003**, *165*, 33.
(59) Horner, O.; Mouesca, J.-M.; Oddou, J.-L.; Jeandey, C.; Nivière, V.; Mattioli, T. A.; Mathé, C.; Fontecave, M.; Maldivi, P.; Bonville, P.; Halfen, J. A.; Latour, J.-M. *Biochemistry* **2004**, *43*, 8815.
(60) Lombard, M.; Houée-Levin, C.; Touati, D.; Fontecave, M.; Nivière, V. *Biochemistry* **2001**, *40*, 5032.
(61) Adams, M. W. W.; Jenney, F. E., Jr.; Clay, M. D.; Johnson, M. K. *JBIC, J. Biol. Inorg. Chem.* **2002**, *7*, 647.
(62) Bou-Abdallah, F.; Chasteen, N. D. *JBIC, J. Biol. Inorg. Chem.* **2008**, *13*, 15.
(63) Nilges, M. J. *SIMPIPM*; University of Illinois: Urbana–Champaign, IL, 2002.
(64) Otwinowski, Z.; Minor, W. *Methods Enzymol.* **1997**, *276*, 307.
(65) Vagin, A.; Teplyakov, A. *J. Appl. Crystallogr.* **1997**, *30*, 1022.
(66) Murshudov, G. N.; Vagin, A. A.; Dodson, E. J. *Acta Crystallogr., Sect. D: Biol. Crystallogr.* **1997**, *D53*, 240.
(67) Emsley, P.; Cowtan, K. *Acta Crystallogr., Sect. D: Biol. Crystallogr.* **2004**, *D60*, 2126.
(68) Adams, P. D.; Afonine, P. V.; Bunkóczi, G.; Chen, V. B.; Davis, I. W.; Echols, N.; Headd, J. J.; Hung, L. W.; Kapral, G. J.; Grosse-Kunstleve, R. W.; McCoy, A. J.; Moriarty, N. W.; Oeffner, R.; Read, R. J.; Richardson, D. C.; Richardson, J. S.; Terwilliger, T. C.; Zwart, P. H. *Acta Crystallogr., Sect. D: Biol. Crystallogr.* **2010**, *66*, 213.